Grant Agreement Number & Project Short Name:
23FUN08 - MetSuperQ

Deliverable Reference Number and Title:
D1 - Report on scanning probe methods working at mK temperatures and dedicated design and fabrication processes of qubits to elucidate decoherence processes

Organisation name of the lead participant for the deliverable:
Eidgenössische Technische Hochschule Zürich, ETHZ

Due date of the deliverable:
31 January 2026

Actual submission date of the deliverable:
1 February 2026

Confidentiality Status: PU - Public, fully open (remember to deposit public deliverables in a trusted repository)

Deliverable Cover Sheet

Funded by the European Union. Views and opinions expressed are however those of the author(s) only and do not necessarily reflect those of the European Union or EURAMET. Neither the European Union nor the granting authority can be held responsible for them.

The project has received funding from the European Partnership on Metrology, co-financed from the European Union's Horizon Europe Research and Innovation Programme and by the Participating States.

TABLE OF CONTENTS

1 Summary 3
2 Introduction 3
3 Defined qubit designs and fabrication processes 4
3.1 Transmon qubits for studying specific known decoherence mechanisms 4
3.2 In-situ stencil mask assisted transmon qubit 5
3.3 Transmon qubits for interlaboratory and reproducibility testing 6
3.4 Fluxonium qubits for interlaboratory and reproducibility testing 8
4 DC and RF scanning SQUID magnetometer setup working at sub 1 K temperatures 10
5 SMM setup working at mK temperatures 11
6 SGM imaging of live superconducting circuits 11
7 Best practice guidance on building experimental setups for Tantalum qubits 12
8 References 14
9 Table of Abbreviations 15
9.1 Institutions 15
10 Attachment 1: Publication Preprint 15

1 Summary

This deliverable reports on initial activities in work package WP1 for systematic decoherence studies in superconducting qubits.

The consortium has designed and fabricated standardised transmon and fluxonium qubit devices for interlaboratory comparison and reproducibility testing, as well as qubit samples for investigating specific decoherence mechanisms.

To enable detailed characterization of these superconducting devices, novel scanning probe microscopy methods are being developed. Progress has been made on millikelvin scanning probe instrumentation, with several low-temperature systems having been installed or upgraded. Scanning SQUID and scanning microwave microscopy capabilities down to 50 mK are being developed, incorporating a travelling wave parametric amplifier (TWPA) for sensitive and high-frequency measurements. Notably, a scanning gate microscope achieved the first direct imaging of individual two-level system defects in live superconducting circuits.

As part of evaluating high-coherence materials for superconducting qubits, quasiparticle tunnelling in tantalum versus niobium qubits was investigated, finding tantalum more sensitive to infrared radiation but demonstrating that appropriate filtering and shielding suppress quasiparticle generation to negligible levels. This work provides practical guidelines for experimental setups using tantalum-based devices.

These activities lay the groundwork for the detailed materials characterization relevant for the subsequent project activities.

2 Introduction

This deliverable is the combined output of the initial activities in the work package WP1 of the MetSuperQ project. The aim of this work package is to investigate new ways for the metrological characterisation of materials used for superconducting qubits, at temperatures below 1 K. This includes exploring different high-coherence materials, qubit circuit designs, and processing steps to facilitate comparisons of material measurement techniques. Suitable scanning probe microscopy techniques are used in addition to standard qubit measurements to characterise the resulting devices, allowing for feedback in optimizing material and design parameters. In addition, this work package aims to develop standardised design and processing procedures for interlaboratory comparisons and reproducibility tests of material measurement techniques. The initial activities reported in this deliverable have laid the foundation for all four tasks of WP1 and also feed into other work packages as described in the following.

As part of task 1.1, we have conducted design and fabrication work that is the basis for interlaboratory comparisons and reproducibility tests in other work packages, and we have worked on the design and fabrication of qubit samples for investigating decoherence mechanisms. This work corresponds to activities A1.1.1–A1.1.3 and is reported in Section 3.

In tasks 1.2 and 1.3, the consortium aims to characterise qubit devices and materials at low frequencies and at microwave frequencies using scanning probe microscopy techniques. The consortium works on a variety of techniques including scanning microwave microscopy (SMM) and scanning superconducting quantum interference device (SQUID) microscopy (SSM) imaging of current flows, magnetic flux, and dissipation in superconducting qubit devices of various designs and material compositions. In Section 4, we report on developing a scanning SQUID magnetometer setup working at temperatures below 1K, see activities A1.2.2–A1.2.4. Furthermore, we report on an upgrade of the capabilities for SMM to work at millikelvin temperatures according to activities A1.2.2–A1.2.4 in Section 4. A new scanning gate microscope (SGM) operating at millikelvin temperature is reported along with measurement results on SGM imaging of live superconducting circuits in Section 5, and is presented in more detail in the recent publication [Hegedus2025]. This corresponds to parts of the activities A1.1.2 and A1.3.3.

One of the aims of WP1 is to evaluate materials for high-coherence superconducting qubits (task 1.4), including Tantalum, which is a promising candidate for base metallization or the Josephson junctions of superconducting qubit devices. However, the smaller superconducting energy gap compared to Niobium, makes Tantalum more susceptible to quasiparticle tunnelling, requiring mitigation strategies against the generation of

quasiparticles. We have used dedicated quantum devices that are highly sensitive to quasiparticle tunnelling as a metrological tool to characterise quasiparticles tunnelling in an experimental setup. Using these devices, we have investigated the effect of, e.g., infrared filtering and infrared absorption in line with activity A1.4.1. The resulting best practices guidance for building experimental setups that allow the characterisation of Tantalum qubits without being limited by quasiparticle tunnelling is summarized in Section 7 and described in detail in a publication preprint attached to this report.

3 Defined qubit designs and fabrication processes

In this section, we report on the design and fabrication work conducted in the initial phase of the project. On the one hand, the consortium has designed and fabricated transmon samples that are the basis for studies on specific decoherence mechanisms. On the other hand, samples with multiple qubit types have been fabricated for interlaboratory comparisons and reproducibility tests.

3.1 Transmon qubits for studying specific known decoherence mechanisms

To study decoherence mechanisms, ETHZ has defined a minimalistic baseline design that aims at suppressing known decoherence mechanisms. The design was inspired by previous reports of transmon qubits with coherence times greater than 200 µs, which have used single-junction, two-island designs with a long dimension of approximately 1 mm [Place2021], [Kono2024], [Wang2022]. Since the surface energy participation ratio of transmon qubits scales inversely with their size [Dial2016], larger transmons are expected to have reduced losses from coupling to lossy interfaces.

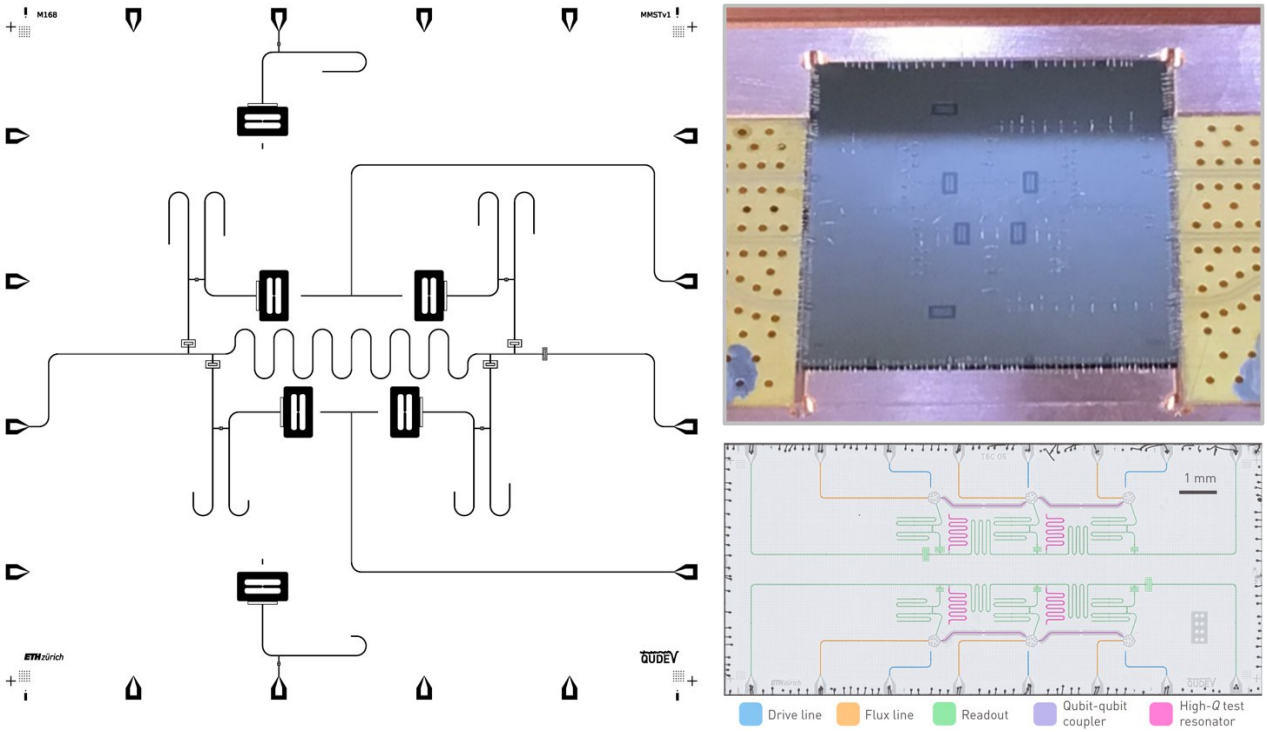


Figure 1 (left) Design of a quantum device with four fixed-frequency transmons with large capacitor pads, coupled to a common feedline for multiplexed readout and to two multiplexed charge lines. The design includes additional test structures at the top and bottom. *(top right)* Fabricated sample of the four-qubit design, wire-bonded to a printed circuit board. *(bottom right)* False-color micrograph of a qubit sample of an alternative baseline design with more similarity to quantum devices used in quantum information processing experiments.

The design is based on two pads of 750 µm by 125 µm, separated by 50 µm and with 150 µm of spacing to the ground plane on all sides. Using fixed-frequency transmons (around 5 GHz) with a single Josephson junction avoids sensitivity to flux noise, and the absence of a flux control line removes a potential decay channel that is present on devices with flux-tunable transmons. We have designed weakly-coupled charge control lines, which set limits to the relaxation time at up to 4 ms. This limit dominates over the Purcell limit of beyond 10 ms from the readout circuitry, which consists of a weakly-coupled (80 MHz), far-detuned readout resonator with a resonance around 1 GHz above the qubit frequency and a Purcell filter.

On a sample of 14 mm by 14 mm, we have placed four qubits with individual readout resonators and Purcell filters, coupled to a shared feedline for frequency-multiplexed readout, see Figure 1 (left). We use multiplexed charge control with two charge lines controlling a pair of qubits each. The design does not include any direct coupling between qubits. To minimize the number of fabrication steps that could potentially reduce the quality factors, e.g., due to contamination with resist residues, the baseline design is meant to be fabricated without any airbridge crossovers. To this end, the feature placement is made compatible with ground plane connections by wire bonds.

ETHZ has fabricated samples of the base line design on a high-resistivity intrinsic silicon substrate with a fabrication process similar to the one described in [ColaoZanuz2025] using oxygen-plasma post-development cleaning. In this process, we have defined signal lines, resonators, and qubit islands by structuring the Nb base metallization layer using photolithography and reactive ion etching. After dicing the wafer, we have fabricated Al/AlOx/Al Josephson junctions on chip scale using electron-beam lithography and two-angle shadow evaporation. Aluminum bandages to connect the junctions with the base metallization are deposited in an additional electron-beam lithography step.

For the planned characterization in a cryogenic measurement setup, the samples are wire-bonded to a printed circuit board mounted on a copper base, see Figure 1 (top right), and covered with an aluminum lid to provide light-tightness. After an initial characterization, the samples will serve as a tool for studying decoherence mechanisms. Comparison to further samples where single parameters of the design or the fabrication process are varied will allow us to quantify the effects of such variations on qubit coherence. Moreover, samples of the same design can be fabricated with a different material combination to study high-coherence materials for superconducting qubits.

While simplified test devices as described above can be used to study particular decoherence mechanisms, some of the design choices reported above can be in conflict with design criteria for large-scale qubit devices for quantum information processing, e.g., due to space constraints or due to the need for fast qubit control. To bridge this gap, ETHZ has defined a second baseline design similar to quantum devices used for high-level experiments, such as quantum error correction experiments [Krinner2022]. This design contains two chains of three flux-tunable transmon qubits each, with inter-qubit coupling and multiplexed readout in each chain, and with individual charge lines, flux lines, readout resonators, and Purcell filters for each qubit, see the false-color micrograph in Figure 1 (bottom right). In a recent related study [ColaoZanuz2025], samples of this design were used to study the influence of the junction area on the spectral density of two-level system (TLS) defect modes as well as the influence of post-development cleaning on quality factors. In the context of MetSuperQ, this design could help to verify insights from the experiments on large-transmon samples in a setting that is closer to realistic use cases of superconducting qubits. The use of the second baseline design within the scope of the project is conditioned on what insights are gained in the experiments on the large-transmon samples.

3.2 In-situ stencil mask assisted transmon qubit

DFM made initial designs of stencil masks suitable for in-situ transmon qubit fabrication. These first designs are now being tested and simulated, after which fabrication will take place. Once produced, KU will together with DFM measure these devices with the aim of testing improved performance due to avoiding the issues typical for resist-based fabrication.

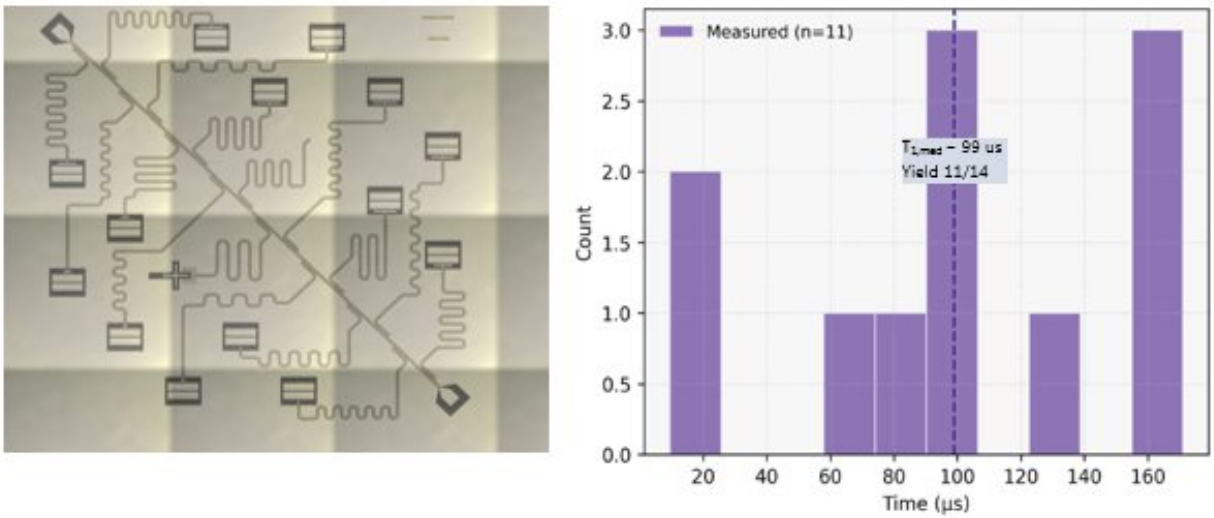


Figure 2 Layout and fabrication of a 14 qubit feedline driven reference chip and low temperature T1 characterization measurements.

In order to prepare for measurements on qubits produced in the project, notably the transmons produced by DFM through stencil-mask-assisted fabrication, KU has focused on setting up a qubit characterization setup and measurement protocols using conventionally fabricated transmons. Design and fabrication of two types of in-house fabricated chips have been established, one with 5 coupled flux-tunable transmons (surface code parity configuration) and another with 14 fixed frequency qubits. Both chips are made on highly resistive Si wafer with Al based Josephson junctions and ground plane. The resonators are inductively coupled to the feedline and capacitively coupled to the two-pad transmons. The 14 feedline-driven fixed frequency qubits are made to monitor the chip-chip fabrication process as well as the spread in coherence times (Q factor) across the chip. Initial measurements yield e.g. T1 with an average around 99 us and the highest T1 of ~170 us (yield 11/14).

The 5-qubit flux-tunable transmon chip allows for two-qubit interactions with design coupling of around 10MHz. Two-qubit measurements have been initiated with observation of coherent oscillation between the 11-20 states and implementation of a Cz gate between two qubits.

3.3 Transmon qubits for interlaboratory and reproducibility testing

NPL has designed and fabricated fixed frequency transmon qubits for use in the MetSuperQ Round Robin intercomparison. These samples, aimed at single qubit benchmarking, have therefore been made small, with only two resonator/qubits per chip, such as to avoid introducing various decoherence processes, crosstalk, etc. that may arise from large scale chips. The fixed frequency of the transmons reduces contribution of flux noise to the decoherence budget and allows to in greater detail explore decoherence from TLS in particular. The layout is shown in Figure 3. In addition to two qubit/readout resonator pairs the chip contains one additional witness resonator that is weakly coupled to the readout transmission line. This resonator is designed to mimic the qubit capacitor dimensions such as to act as a probe of the materials quality with a dielectric and interface participation ratio similar to that of the transmon capacitors. The weak coupling is used to get a more accurate measurement of the resonator's internal quality factor, as a proxy to the expected qubit relaxation time if limited by TLS and materials-level losses.

These samples are made on 7x5 mm sized chips using NPL's standard Aluminium process in the SuperFab cleanroom at Royal Holloway University of London. Readout resonators are coupled to a common feedline for qubit readout, and qubits are controlled through individual qubit control lines. Readout resonators are designed to be in the range f_r=6.5-7.5 GHz, and qubits designed to have the ground to excited energy level transition frequency at f_q=5.0 GHz, with an anharmonicity of -150 MHz. This puts these qubits solidly in the transmon regime, suppressing charge noise and frequency fluctuations from quasiparticle parity switching in the g-e transition, while these decoherence processes can still be accessed through the e-f transition. Further design

parameters, such as control line coupling capacitances, resonator loaded quality factor, and qubit-resonator coupling capacitance were chosen to maximise readout fidelity while maintaining measurement induced QND errors. The Purcell-induced relaxation rate from both control line and resonator coupling & cavity relaxation is estimated to ~6 kHz, equivalent to T_1~170 us. This complements the standardised designs by ETHZ by trading Purcell filters for a more simplified device design, having the bare minimum of components that could also affect the qubit performance. The transmons here utilises the traditional Xmon layout which is known to couple more strongly to TLS and material imperfections and achieving somewhat lower coherence times than e.g. paddle type transmons. However, this amplifies the decoherence contribution from such sources, making them easier to detect through measurements without being masked by other possible sources of decoherence, and thereby allowing for improved understanding and feedback towards mitigating materials-level sources of decoherence.

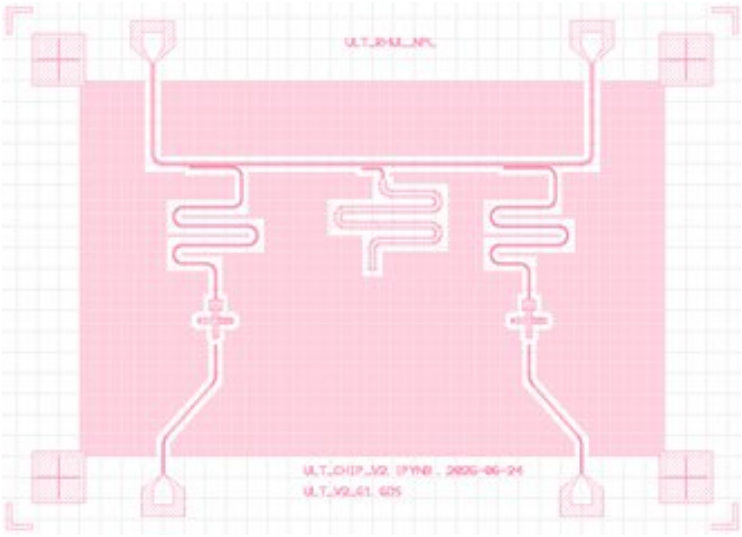


Figure 3 Layout of NPL's 7x5 mm single qubit chip for interlaboratory tests.

NPL has also designed fixed frequency coupled transmon qubits using a cross-resonance coupler. With a similar approach as for the single qubit chip, we here keep the chip size small and limit the number of components on the chip to introduce fewer possible unintended sources of decoherence. Similarly, we here chose a gate architecture that provides simplicity and reduction of potential decoherence sources in the coupler itself. This will allow future studies to easier unpick the specific impact of decoherence processes occurring in the qubits on the two-qubit gate operation. By avoiding flux-tunable components both in qubits an coupler, the aim is to study how the presence of TLS and quasiparticles in particular impacts two-qubit gate operations. For this purpose we have designed a cross resonance gate, which we aim to have a high ZX rate. The cross-resonance gate takes two independent qubits identical to the single qubit design discussed above, and connects the two qubits with a $\lambda/2$ resonator, here designed to have a frequency $f_{coupler}$ = 7.0 GHz. The layout of the chip is shown in Figure 4.

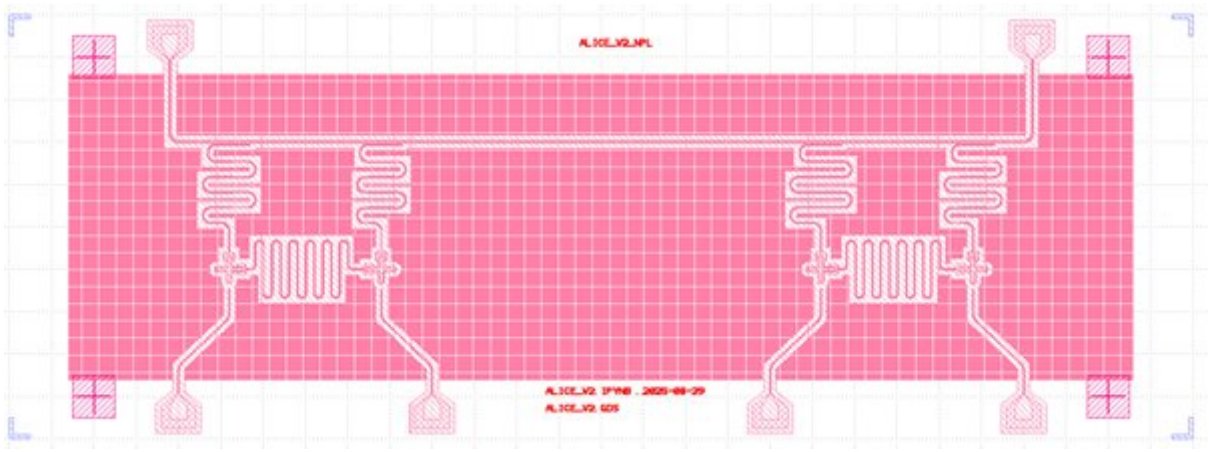


Figure 4 Layout of the NPL 14x5 mm two-qubit coupler chip for interlaboratory and reproducibility testing.

These devices will be used by NPL for the MetSuperQ qubit intercomparison and sent to other participants.

VTT designed and fabricated qubit samples based on Al–AlOx–Nb trilayer Josephson junctions and delivered these to NPL for independent T_1/T_2 benchmarking measurements. These chips are superconducting transmon-type qubit devices incorporating multiple qubit–readout resonator structures enabling frequency-multiplexed readout, with dedicated microwave drive/readout lines and flux-bias lines for flux-tunable elements. The devices are realized using the native-oxide-passivated trilayer junction (NAPA) process described in our publication [Sethi2025], based on Al–AlOx–Nb trilayer Josephson junctions on high resistivity Si, patterned subtractively using optical lithography and RIE, with native Al-oxide sidewall passivation retained to electrically isolate the junction sidewalls without aggressive oxide removal steps.

3.4 Fluxonium qubits for interlaboratory and reproducibility testing

The fluxonium qubit has attracted considerable attention in recent years due to its coherence times in the ms-range [Popp2014, Nguyen2019] and high single- and two-qubit gate fidelities exceeding 99.9% [Rower2024, Ding2023]. A fluxonium qubit is composed of a Josephson junction shunted by a so-called superinductor, which features an impedance larger than the resistance quantum RQ = h / 4e^2 and inductance on the order of 100s of nH. This qubit type features a large tuning range for its qubit transition frequency, and also a anharmonicity of several GHz at its typical flux bias operation point of φ_{ext}=0.5 φ_0. Because of the high impedance of the circuit, the wavefunction of the fluxonium in charge space is highly localized. The effect of charge noise on fluxonium is therefore greatly reduced.

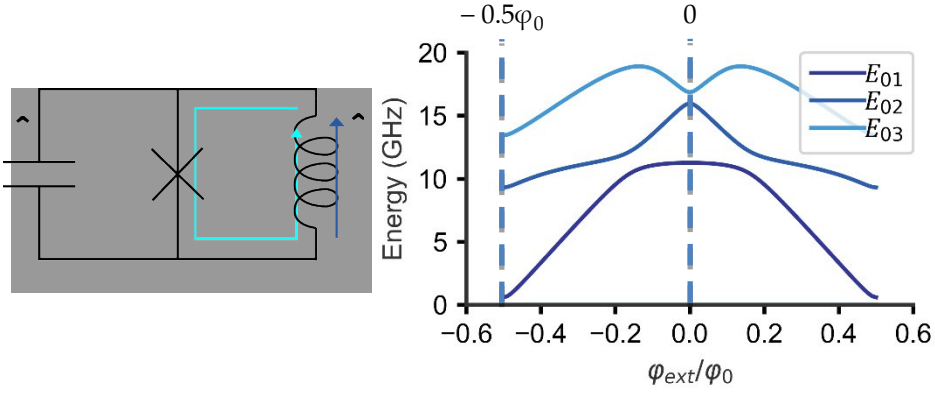


Figure 5 (left) Equivalent circuit of a fluxonium, and typical transition energy spectrum as a function of external flux through the fluxonium loop (right).

For their design PTB has chosen the energies of the three fluxonium building blocks (see Figure 5) as E_J/h=*9.0* GHz, E_C/h=*2.5* GHz, and E_L/h=*1.0* GHz. This leads to a spectrum of the fluxonium as shown in Figure 5 (right).

At no external field ($\varphi_{ext}=0$), the transition frequency of E_{01} is maximal at 11.3 GHz. At the typical operation point of half a flux quantum external field ($\varphi_{ext}=0.5\varphi_0$), the transition frequency E_{01} reaches its lowest value of 0.6 GHz. Fig. 1 (right) also shows the transition frequencies of E_{02} and E_{03} as a function of the external field.

For their interlaboratory testing device PTB has chosen a 9 x 9 mm^2 chip layout with four uncoupled fluxonium-resonator pairs, each with an on-chip flux bias line. The chip design is shown in Figure 6, with the zoom-ins detailing the granular aluminum (grAl) readout resonators coupled to fluxoniums via a shared inductance. In the chip layout overview the Al base layer is shown in white and grAl resonators in light blue. The dimension of the resonator pads are 600 µm x 100 µm, and their spacing is 400 µm. The spacing between resonators and the ground plane is 50 µm and 700 µm from vertical and horizontal sides. The inductor strip has a width of 22.6 µm and a length of 1276 µm to provide the inductance for tuning the readout resonator frequency, while the shared segment coupling fluxonium and resonator has a width of 0.8 µm and a length of 10 µm. We aim for a kinetic inductance of 0.25 nH/square for the 30 nm thick grAl film. The on chip bias line is visible to the left of the fluxonium in the bottom right picture of Figure 6. For implementing the superinductor shunting the small Josephson junction, there are 80 junctions in the junction array. Each of them has an area of 1 µm^2, while the small junction has an area of 0.155 µm^2.

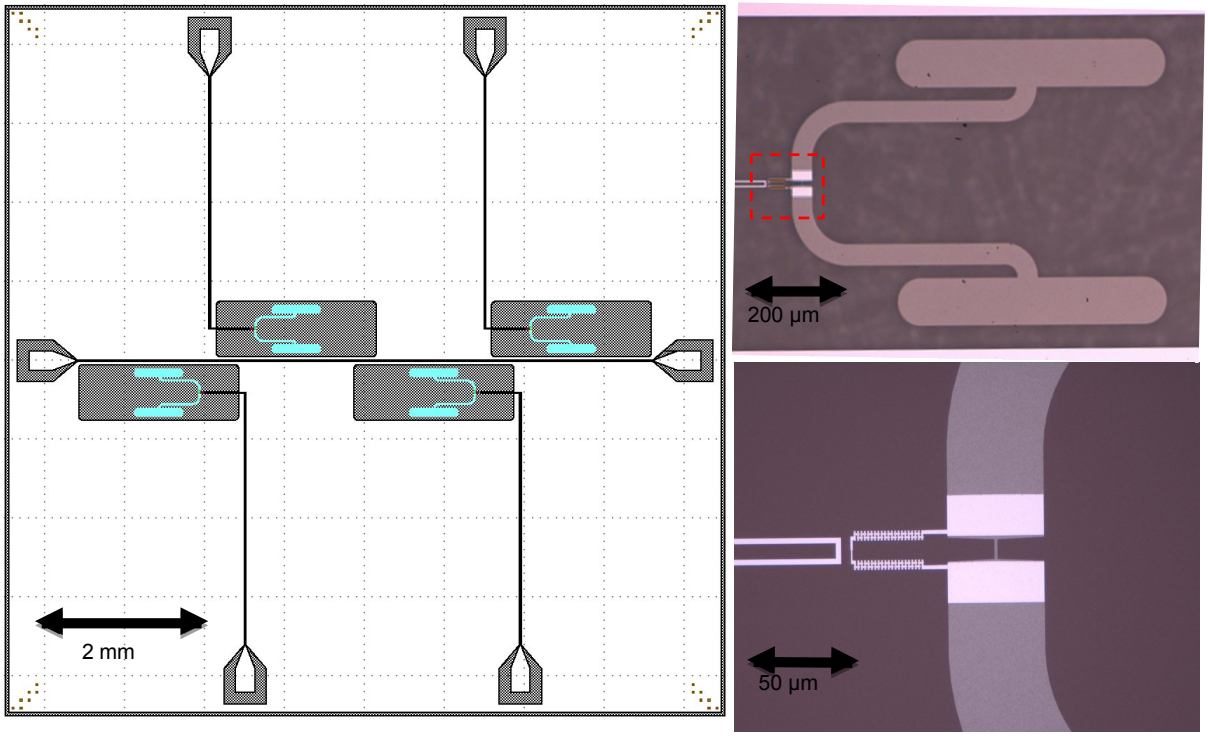


Figure 6 (left) Design of the PTB test device with four fluxoniums each coupled to its own grAl resonator. All resonators are coupled to a common feedline, while each fluxonium has an individual flux line. (top right) Zoom-in on the grAl resonator and a fluxonium. (bottom right) Zoom-in of the red dashed box in the top-right picture, showing a fluxonium and the shared segment of grAl implementing the qubit resonator coupling.

For the fabrication of the device, PTB first evaporate a 30 nm Al base layer on a c-plane sapphire substrate, which prior to film deposition undergoes a rinsing step in acetone followed by 5 min O_2 plasma ashing. The central feed line, cutout for the fluxonium-resonator circuits, and flux lines are patterned using positive lithography and wet etching with MF321 developer. For the grAl resonators patterned in lift-off technique, PTB deposit a 30 nm thick grAl film by evaporating pure Al in an oxygen atmosphere with pressure 1.4E-5 mbar. This typically results in a resistance of 400 Ω/square for 30 nm thickness. Before the evaporation, an O_2 plasma cleaning at a pressure of 30 Pa O2, and 15 W power is performed for a duration of 60 s.

The small junction is patterned using a shadow evaporation again following a oxygen plasma cleaning to remove resist residue. For the final fabrication step another oxygen plasma cleaning with the same parameters is performed. To remove the native Al oxide from the previously deposited Al and grAl films, an argon-milling

is employed. Then a controlled oxidation is performed to form the barrier of the overlap junctions in the junction array, which serve as the superinductor. The final Al layer has 80 nm thickness.

KIT has chosen gradiometric fluxonium devices similar to the ones in [Bénâtre2025]. In contrast to the PTB implementation, the KIT design uses grAl instead of an array of Josephson junctions to implement the superinductance. A selected device was already measured at KIT and delivered to NPL for testing. Measurements at NPL are currently ongoing.

4 DC and RF scanning SQUID magnetometer setup working at sub 1 K temperatures

UNIBAS has been developing scanning probe equipment capable of reaching the target temperatures of 50 mK as specified in tasks A1.2.2 and A1.2.3. The team has been systematically optimizing SQUID-on-tip and SQUID-on-cantilever sensors specifically for operation at millikelvin temperatures, with particular attention to achieving low critical currents and zero-field sensitivity (see Figure 7 a-e). These optimizations are critical for the successful implementation of both low-frequency and radio frequency (RF) scanning magnetometry at sub-1 K temperatures.

Several experimental cooldown attempts were conducted in a 300 mK cryostat using the optimized sensors with the aim of imaging current flow, trapped flux, and potentially dissipation in transmon qubit devices supplied by ETHZ. While these initial attempts encountered cryostat malfunctions, these technical issues have since been resolved. In parallel with these experimental efforts, infrastructure has been established through the installation of a dilution refrigerator that will enable measurements at the target temperature of 50 mK or lower (see Figure 7 f). A scanning probe microscope head (Figure 7 g) is currently being set up within this dilution refrigerator system, with careful attention being paid to implementing effective vibration isolation measures, which are essential for achieving the required measurement precision.

For the RF scanning magnetometry work outlined in A1.2.3, UNIBAS has made initial designs for several implementations of SQUID sensors with integrated RF dispersive read-out capabilities, on cantilever. The first prototypes of these RF-enabled sensors are currently in fabrication.

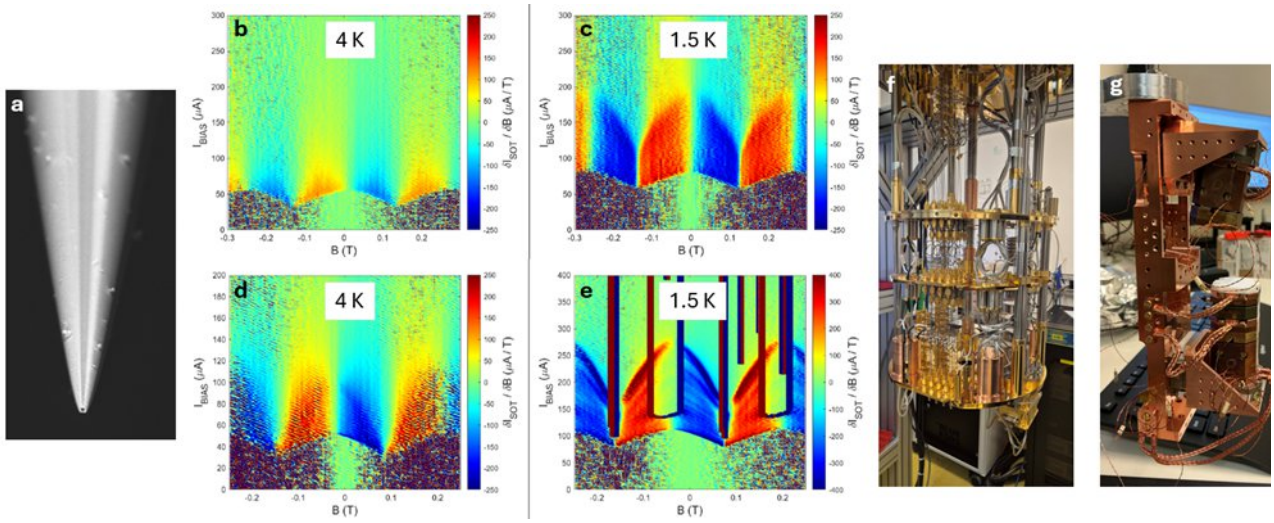


Figure 7 **a** Scanning electron microscopy (SEM) image of an Nb SQUID-on-tip sensor fabricated at UNIBAS. **b – c** Magnetic response dI/dB of an SOT sensor as a function of applied magnetic field and bias current, showing a quantum interference pattern, taken at a temperature of 4 K (**b**) and 1.5 K (**c**). The measurements demonstrate SQUID operation at 1.5 K. **d – e** Similar magnetic response measurements of a second SOT sensor, which displays sensitivity at zero applied magnetic field. **f** Cold plates of mK dilution refrigerator setup, with modifications for scanning probe setup under construction at UNIBAS. **g** Home-built mK scanning probe microscope head that will be used in dilution refrigerator. The scanning probe head is compatible with SSM, SMM, and SGM.

5 SMM setup working at mK temperatures

UNIBAS with the help of METAS has been upgrading its scanning microscopy capabilities to operate at millikelvin temperatures. The same newly installed dilution refrigerator mentioned in the previous section will be used for this task. This cryostat installation has been configured with various high-frequency lines, making it suitable for conducting SMM experiments on transmon qubits.

A flexible scanning microscope head is currently being integrated into the system, designed to accommodate multiple measurement modalities including SSM, SMM, and SGM. Both the SMM and SGM capabilities will be specifically utilized to study TLSs and 1/f charge noise.

To support the SMM measurements, a specialized cryogenic RF setup has been designed and is currently under construction (see Figure 8 a). The RF setup includes a TWPA received from VTT, complemented by additional read-out electronics and a dedicated RF printed circuit board connecting directly to the scanning probe cantilevers. This TWPA provides low-noise amplification essential for sensitive microwave measurements and can alternatively be utilized for qubit read-out operations.

In parallel to the millikelvin system development, UNIBAS and METAS have successfully constructed a 4K SMM setup (see Figure 8 b-c) and are currently taking first scans of samples unrelated to this project. While this setup operates at temperatures too high for the qubit measurements envisioned in this project, it serves as a valuable platform for developing and refining measurement methods, calibration procedures, and data analysis techniques that will be transferred to the millikelvin system once operational.

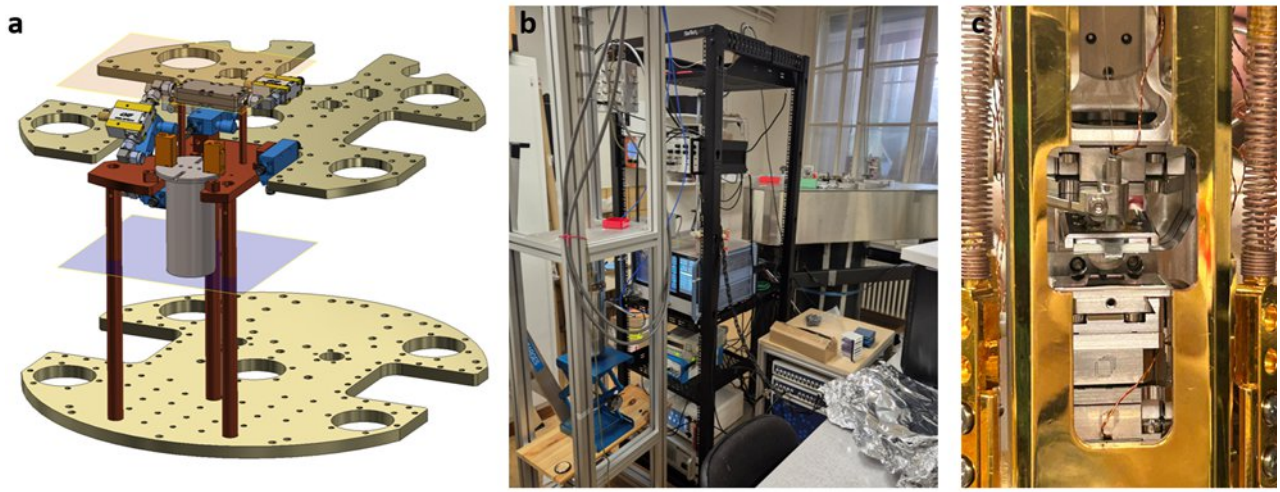


Figure 8 **a** CAD design of high-frequency setup to be integrated in UNIBAS dilution refrigerator. The high-frequency setup incorporates a VTT TWPA and associated electronics, as well as additional electronics suitable for performing low-noise SMM. **b** 4K setup at UNIBAS, with home-built probe dedicated for SMM. Constructed and operated together with METAS. **c** Home-built SMM head used in the 4K setup of **b**.

6 SGM imaging of live superconducting circuits

NPL has been developing a new scanning probe microscope to locate and study individual TLS defects in live quantum circuits at millikelvin temperatures. The mK SGM can unravel the detailed microscopic nature and chemical origin of TLS defects, directing targeted strategies for their eventual mitigation and improve device coherences. Even after five decades since TLS defects were postulated to explain the macroscopic behaviour of glassy systems, their origin, location and properties remain unknown – an issue that has gained urgency in recent years due to their detrimental effects on the coherence and noise of solid-state quantum devices. As even a single TLS can spoil the performance of an entire quantum circuit, they pose one of the biggest roadblocks limiting qubit fidelity and the scaling up of quantum processors beyond fault tolerance. As the extremely low energy scales of TLS (~meV) render them impervious to much of traditional condensed matter probes, we developed a novel instrument combining scanning probe microscopy with circuit quantum

electrodynamics techniques to study them. By mapping and visualizing the most detrimental TLS in the bath coupling to the circuit, we pinpointed the dominant sources of ubiquitous 1/*f* dielectric noise and energy relaxation in quantum circuits. The SGM also allows to deduce the three-dimensional orientation of individual TLS electric dipole moments. Figure *9* shows the mK SGM setup (a-e), as well as SGM scans of single TLS.

The mK SGM approach could enable targeted fabrication strategies, to locations where the most detrimental TLS are found, and present a new way to investigate the assumptions underpinning our current understanding of decoherence in superconducting quantum circuits. Details of TLS imaging and the SGM setup can be found in the published paper [Hegedus2025].

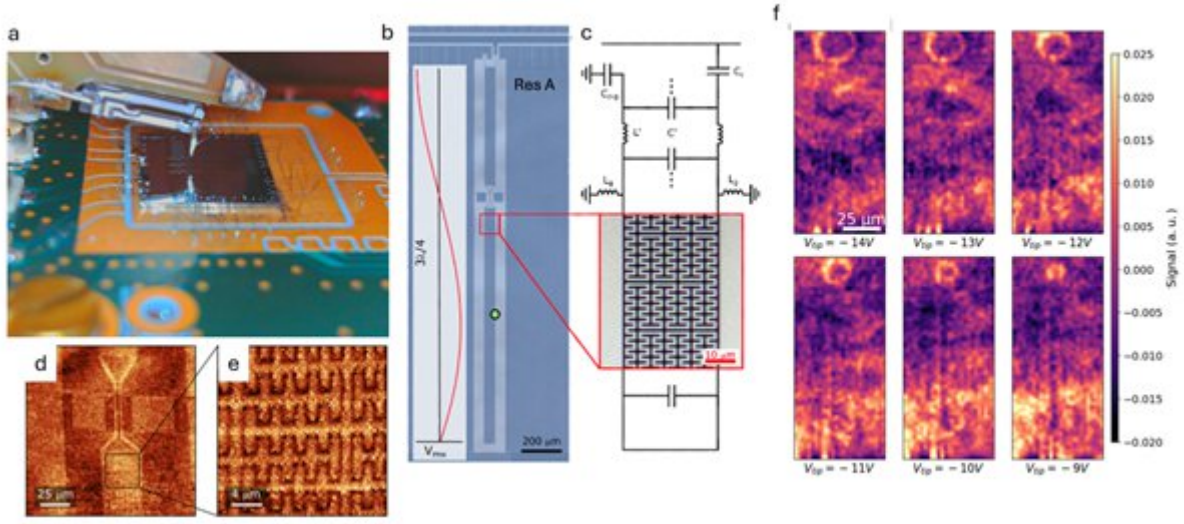


Figure 9 (a) The setup for performing SGM on live quantum circuits. (b) optical image of the resonator studied, with its equivalent circuit representation in (c). (d-e) are atomic force microscopy topography scans of the live resonator at millikelvin showing the features highlighted in (b) and (c). Panels in (f) show the data where a TLS defect was located for the first time after fifty years of studying them. At the centre of the circular contour near the top of each panel sits a TLS defect. The details of the measurement are in our paper [Hegedus2025].

7 Best practice guidance on building experimental setups for Tantalum qubits

ETHZ has investigated quasiparticle tunnelling in offset-charge-sensitive transmon qubits fabricated with either niobium or tantalum as base metallization, using otherwise identical device designs and junction fabrication processes. With a charge dispersion of several MHz, the devices are suitable to resolve individual charge-parity switching events, and can act as sensitive probes of nonequilibrium quasiparticles for quantitative assessment of quasiparticle generation mechanisms in realistic cryogenic environments. The influence of infrared radiation on quasiparticle tunnelling rates was studied by introducing a controlled thermal radiation source and by modifying the radiative environment of the qubits. The measurements reveal that tantalum-based devices exhibit both higher background tunnelling rates and a stronger sensitivity to infrared radiation than their niobium counterparts, indicating that tantalum qubits are more readily limited by radiatively generated quasiparticles in typical superconducting qubit setups. At the same time, it was demonstrated that appropriate mitigation measures can suppress tunnelling rates to levels that are no longer relevant for qubit coherence. The findings are reported in a publication preprint (attached to the report) and summarized below. Based on these findings, several practical principles emerge for designing experimental setups intended for tantalum-based superconducting qubits, where mitigation of infrared radiation must be treated as a central design requirement.

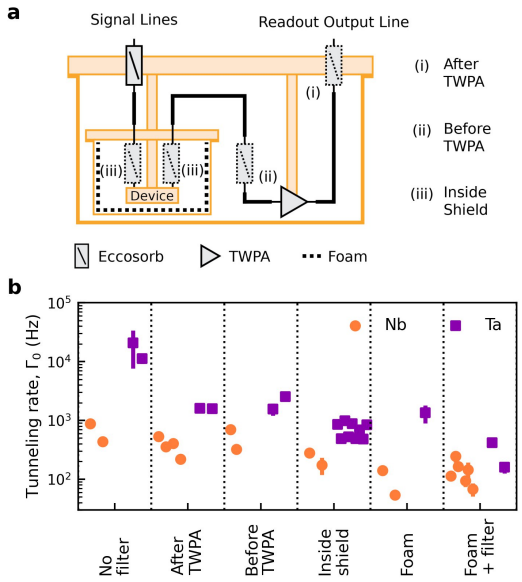


Figure 10 Suppressing infrared radiative background through in-line filters and infrared-absorbing foam. (a) Schematic of the experimental setup. Eccosorb filters are placed at three positions along the readout output lines and signal lines, before and after the TWPA. All filters are thermally anchored to the base temperature plate using copper braids (not shown in the schematic). Eccosorb foam is placed inside the shield assembly. (b) Tunnelling rates from multiple measurements are compared for six filter and foam configurations, for niobium-based and tantalum-based devices.

In our experimental setup, the volume below the dilution refrigerator's mixing chamber plate is copper-shielded against radiation from higher-temperature stages. Inside this region, devices are mounted following an additional box-in-box strategy: an intermediate shield assembly provides further protection against spurious radiation and fields, and the samples are enclosed in a centimeter-sized, innermost copper cavity with aluminum lid. This cavity houses only the silicon chips and the printed circuit board with soldered cable connectors. The setup is illustrated in Figure 10 (a).

As a best practice recommendation, all signal lines as well as output lines leading to the sample package must be protected with in-line infrared filters. The placement of these filters at different positions was investigated, specifically inside the intermediate shield assembly, and on either side of the TWPA. The configuration where filters are placed as close as possible to the quantum device and, in particular, inside the cold shield volume and thermalized with the base temperature plate, yielded the lowest tunnelling rates, as shown in Figure 10 (b) (first four columns). This way, the filters can block radiation propagating along the cables after entering the cryogenic environment.

Second, ambient infrared radiation inside the shielding must be mitigated independently. As detailed in the attached preprint, we observed that the use of Eccosorb foam inside the sample shield significantly reduces tunnelling rates (see last two columns in Figure 10 (b)), demonstrating that both in-line and free-space IR radiation within nominally shielded volumes can be dominant quasiparticle sources. This also highlights the importance of light-tight packaging and careful treatment of seams, connectors, and feedthroughs.

Finally, tunnelling rates were observed to decrease slowly over days after cooldown (see attached preprint), emphasizing that poorly thermalized components can act as long-lived radiative sources and should be minimized through appropriate material choice, mechanical design, and thermal anchoring. Taken together, our findings on shielding, filtering, absorption of free-space radiation, and thermalization define a set of best practices that allow tantalum qubits to be characterized and operated without being fundamentally limited by quasiparticle tunnelling.

8 References

[Benatre2025] D. Bénâtre, et al., "Simultaneous sweet-spot locking of gradiometric fluxonium qubits", Physical Review Applied 24, 054031 (2025). https://doi.org/10.1103/PhysRevApplied.24.054031

[ColaoZanuz2025] D. Colao-Zanuz, et al., "Mitigating losses of superconducting qubits strongly coupled to defect modes", Physical Review Applied 23, 044054 (2025). https://doi.org/10.1103/PhysRevApplied.23.044054

[Dial2016] O. Dial, et al., "Bulk and surface loss in superconducting transmon qubits", Superconductor Science and Technology 29, 044001 (2016). https://doi.org/10.1088/0953-2048/29/4/044001

[Ding2023] L. Ding, et al., "High-Fidelity, Frequency-Flexible Two-Qubit Fluxonium Gates with a Transmon Coupler", Physical Review X 13, 031035 (2023). https://doi.org/10.1103/PhysRevX.13.031035

[Hegedus2025] M. Hegedüs, et. al., “In Situ Scanning Gate Imaging of Individual Quantum Two-Level System Defects in Live Superconducting Circuits”, Science Advances, Vol 11, Issue 18 (2025). https://www.science.org/doi/10.1126/sciadv.adt8586

[Kono2024] S. Kono, et al., "Mechanically induced correlated errors on superconducting qubits with relaxation times exceeding 0.4 ms", Nature Communications 15, 3950 (2024). https://doi.org/10.1038/s41467-024-48230-3

[Krinner2022] S. Krinner, et al., "Realizing repeated quantum error correction in a distance-three surface code", Nature 605, 669–674 (2022). https://doi.org/10.1038/s41586-022-04566-8

[Nguyen2019] L. B. Nguyen, et al., "High-Coherence Fluxonium Qubit", Physical Review X 9, 041041 (2019). https://doi.org/10.1103/PhysRevX.9.041041

[Popp2014] I. M. Pop, et al., "Coherent suppression of electromagnetic dissipation due to superconducting quasiparticles", Nature 508, 369–372 (2014). https://doi.org/10.1038/nature13017

[Place2021] A. P. M. Place, et al., "New material platform for superconducting transmon qubits with coherence times exceeding 0.3 milliseconds", Nature Communications 12, 1779 (2021). https://doi.org/10.1038/s41467-021-22030-5

[Rower2024] D. A. Rower, et al., "Suppressing counter-rotating errors for fast single-qubit gates with fluxonium", PRX Quantum 5, 040342 (2024). https://doi.org/10.1103/PRXQuantum.5.040342

[Sethi2025] P. Sethi, et al., "Native-oxide-passivated trilayer junctions for superconducting qubits", Physical Review Applied 24, 064056 (2025). https://doi.org/10.1103/tblt-589d

[Wang2022] C. Wang, et al., "Towards practical quantum computers: transmon qubit with a lifetime approaching 0.5 milliseconds", npj Quantum Information 8, 3 (2022). https://doi.org/10.1038/s41534-021-00510-2

9 Table of Abbreviations

RF	Radio Frequency	SSM	Scanning SQUID Microscopy
SEM	Scanning Electron Microscopy	SQUID	Superconducting Quantum Interference Device
SGM	Scanning Gate Microscopy	TLS	Two-Level System
SMM	Scanning Microwave Microscopy	TWPA	Travelling-Wave Parametric Amplifier

9.1 Institutions

PTB	Physikalisch-Technische Bundesanstalt	KU	Kobenhavns Universitet
DFM	Dansk Fundamental Metrologi A/S	Orange QS	Orange Quantum Systems Operational B.V.
INRIM	Istituto Nazionale di Ricerca Metrologica	ETHZ	Eidgenössische Technische Hochschule Zürich
JV	Justervesenet	METAS	Eidgenössisches Institut für Metrologie METAS
LNE	Laboratoire national de métrologie et d'essais	NPL	NPL Management Limited
VTT	Teknologian tutkimuskeskus VTT Oy	UNIBAS	Universitat Basel
KIT	Karlsruher Institut fuer Technologie		

10 Attachment 1: Publication Preprint

A preprint for a planned publication about the impact of infrared radiation on Tantalum- and Niobium-based superconducting quantum devices is attached to this report.